Experimental investigation of the mechanical performance of novel rigid connections in prestressed circular composite precast concrete columns under cyclic lateral loading

Journal of Building Engineering 89 (2024) 109150

Contents lists available at ScienceDirect

Journal of Building Engineering

journal homepage: www.elsevier.com/locate/jobe

Experimental investigation of the mechanical performance of novel rigid connections in prestressed circular composite precast concrete columns under cyclic lateral loading

Caiwei Xu [a,b], Le Li [c], Saeed Miramini [a], Lihai Zhang [a,*]

[a] Department of Infrastructure Engineering, The University of Melbourne, VIC, 3010, Australia
[b] Jianke Architectural Design Institute of Guangdong Province, Guangzhou, 510640, China
[c] Institute for Sustainable Industries & Liveable Cities, Victoria University, Footscray, VIC, 3011, Australia

ARTICLE INFO

Keywords:
Composite precast concrete columns
Rigid connections
Cyclic lateral loading test
Seismic performance
Moment-resisting frames
Lateral-force-resisting system

ABSTRACT

The present study introduces an advanced design of Prestressed Circular Composite Precast Concrete Columns (PCCPCCs), which have been applied in real-world structures, equipped with two novel rigid connection types (*i.e.,* the reinforcing-cage connection and the welded-plate connection) to address existing challenges in the design, construction, and quality control of traditional precast concrete (PC) columns. Five full-scale specimens were experimented individually to assess the mechanical performance of PCCPCCs subjected to cyclic lateral loading and constant axial loading. The results indicate that the specimens exhibited no signs of collapse or loss in axial load capacity during the tests. Furthermore, all specimens met or exceeded the performance criteria set by relevant standards, such as GB50011-2010 and ACI 374.1-05, regarding drift ratio, moment capacity, energy dissipation, and ductility. It demonstrates that the novel design of PCCPCCs proposed in this study can be integrated into practical construction projects designed as lateral-force-resisting systems, such as moment-resisting frames and bridges, to accommodate diverse construction project requirements.

Notation

P	axial load at the top-end of specimens
L	lateral load at the top-end of specimens
H	height from the lateral load to the foundation
Δ	lateral displacement at the top-end of specimens
ACR	axial compression ratio
A_{pipe}	area of the cross-section of the pipe
$A_{core\ concrete}$	area of the cross-section of the core concrete
$f_{c,pipe}$	designed concrete compressive strength for the pipe
$f_{c,core\ concrete}$	designed concrete compressive strength for the core concrete
Δ_y	yield displacement
L_y	corresponding lateral loads at yield displacement

* Corresponding author.
E-mail address: lihzhang@unimelb.edu.au (L. Zhang).

https://doi.org/10.1016/j.jobe.2024.109150
Received 10 November 2023; Received in revised form 6 March 2024; Accepted 25 March 2024
Available online 9 April 2024

+	positive direction (towards the west in this paper's experiments)
-	negative direction (towards the east in this paper's experiments)
$M_{p-\Delta}$	moment considering $p-\Delta$ effect
M_{cr}	Cracking moment
β	relative energy dissipation ratio
A_h	area of the hysteresis loop
E1, E2	absolute values of the peak lateral loads of a loop in the positive and negative directions
θ_1', θ_2'	values used to calculate the energy dissipation ratio
Δ_p, L_p	displacement and lateral loads at the peak of a loop
$K_{initial}$	stiffness of the first loop
μ	ductility factor
Δ_u	ultimate displacement
μ_{avg}	average ductility factor

1. Introduction

Precast concrete (PC) structures have recently become popular due to their ability to reduce construction time and waste [1,2], making them more environmentally friendly than traditional cast-in-situ concrete structures [3]. Moreover, precast concrete can be used in modular buildings, which speeds the construction efficiency [4,5]. Conventionally, the elements in PC structures are customized for specific construction projects. The non-standard manufacturing process of PC elements is costly and time-consuming. Further development is, therefore, needed for PC structures to increase their standardization.

As a common element of the PC structure, PC columns are assembled in situ by connecting them to joints or foundations through various connections. Traditionally, grouted sleeve connections, which are classified according to sleeve types consisting of whole grout sleeve and grout sleeve with mechanical splicing end, are used [2]. The detailed construction procedure can be found in JGJ 355–2015 [6]. For this design, the space between the sleeve and the steel bar is only around 10 mm due to the diameter difference. Such low spaces increase the difficulties in the construction and quality inspection process. Additionally, it is difficult to determine whether the grouting material meets the required compressive strength due to the small grouting volume and challenging inspection/in-situ testing procedure [2]. The construction expenses of such a column are also high [2].

Because of the above limitations, a new type of precast column, a Prestressed Circular Composite Precast Concrete Column (PCCPCC), and two innovative connections have been developed as shown in Fig. 1(a), (b), and (c). This new design has the following benefits compared to the previous traditional design. To begin with, the manufacturing of PCCPCCs is more time-saving and sustainable than the conventional precast concrete columns since it is assembled by standardized precast concrete pipe and cast-in-situ concrete core. A detailed introduction of the precast concrete pipe and PCCPCCs can be found in Section 1 and Section 2.1 in Xu et al. [3] and Fig. 3 in this paper. Moreover, as Xu et al. [1] discussed, the pipe contributes to the fire resistance, reinforcement, and capacity of the PCCPCCs. Therefore, with such effective contributions of the pipe, PCCPCCs achieve the goal of standardization in precast element manufacture.

The reinforcing cage used in the reinforcing-cage connection in Fig. 1 (b) is assembled through the hollow section of the pipe, formed by connection-reinforcing bars and connection stirrups. In traditional design, the reinforcing cage runs throughout the column, but this has been modified because of the contribution of reinforcing rebars in the pipe. This modification reduces the cost and increases the constructability of the column. This reinforcing cage connection can also connect the upper or lower end of columns to joints or foundations. The welded-plate connection in Fig. 1 (b) is assembled by welding the connection plate to the PCCPCC plate. This welded steel plate connection is used between the lower end of columns and joints/foundations. When the precast pipe is manufactured in the factory, a steel plate is attached to each end (Pipe-plate in Fig. 1(b)). The welded-plate connection utilizes this feature of the pipe and makes the manufacture of the connection cost-effective. Moreover, constructing the two rigid connections is more convenient than the traditional one. In further application of PCCPCCs under these two rigid connections, the various numbers or strength of the connection-rebars, connection-stirrups, or strength of concrete core can achieve multiple strength requirements in different construction projects.

The mechanical performance of structure components and connections is essential to study whether the novel types of components or connections can be applicable in practical use. Research on the connection of precast components has been popular in recent years because connection relates to the mechanical performance of precast elements and structures, such as the studies by Hu et al. [7]. The cyclic lateral loading test commonly determines this mechanical performance. It is to simulate the cyclic lateral loads that structures in practical application are always subjected to, for example seismic loads or wind loads [8]. For example, Guan et al. [9] conducted a new UHPC-shell strengthened prefabricated concrete column (USPCC) to figure out the impact of the UHPC shell on the prefabricated concrete, where the cyclic loading test was adopted as the experiment method. They stated that the UHPC shell can transfer the damages in the USPCC away from its pedestal joint zones. However, no experiments were carried out on this novel type of PCCPCCs under these two innovative rigid connections.

The study investigates the mechanical performance of PCCPCCs connected to the foundation under the reinforcing-cage connection or through the welded-plate connection. Lab works are designed to simulate the mechanical performance of PCCPCCs under cyclic lateral loading tests, five full-scale specimens were experimented. The failure patterns of PCCPCCs after being loaded and discussions

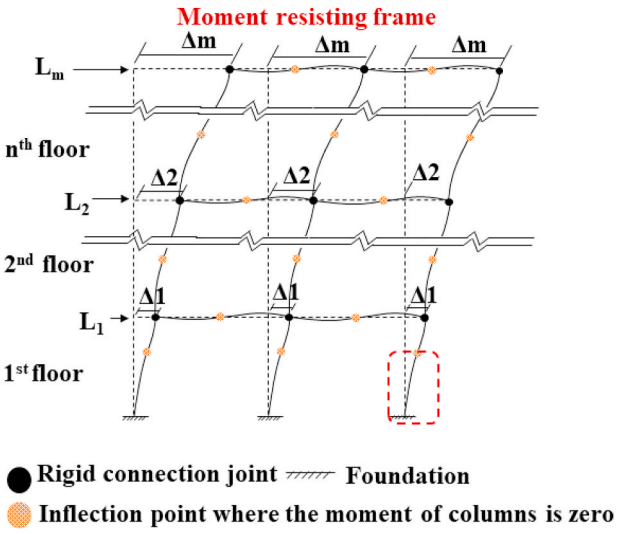

(a)

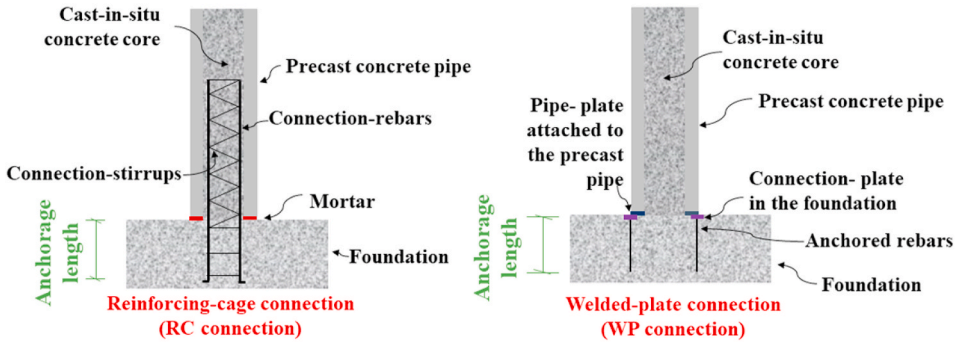

(b)

(c)

Fig. 1. Example of application Prestressed Circular Composite Precast Concrete Columns (PCCPCCs) in the moment resisting frame. (a) Example of application of PCCPCC with rigid connection in moment resisting frame, (b) Details of the rigid connection using reinforcing-cage connection (RC connection), and details of the rigid connection using welded-plate connection (WP connection), (c) PCCPCCs applied as columns at the Qingyuan campus.

of lateral load capacity, drift ratio, moment capacity, energy dissipation, and ductility are obtained in this paper. This research gives the support and guide to the engineers on the design of PCCPCCs. Moreover, the applications of the novel column are adopted in real-world structures, for example, the dining hall at the Qingyuan campus in Fig. 1 (c).

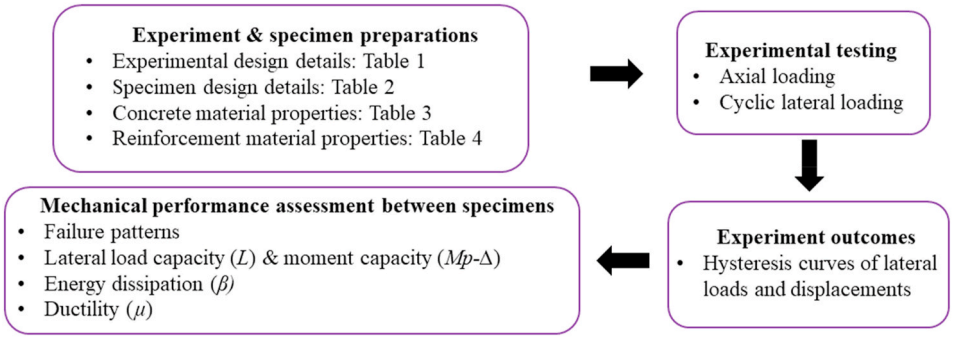

Fig. 2. Experimental methodology of investigation of mechanical performance of PCCPCCs under two types of rigid connection.

2. Methodology

2.1. Framework

Fig. 2 addresses the methodology framework of this study, where the experiment and specimen preparations, experimental testing, experiment outcomes, and mechanical performance assessment were conducted.

2.2. Specimen design

As s shown in Table 1, specimens vary in connection type (RC connection V.S. WP connection), size (diameter in 600 mm V S. 500 mm), and axial loading (3000 kN V S. 500 kN). Fig. 1 (b) shows that PCCPCC consists of two standardized products: a prestressed precast concrete pipe (Fig. 3) manufactured based on JGJ/T 406–2017 [10] and cast-in-situ concrete manufactured based on GB/T14902-2012 [11].

2.2.1. Details of prestressed precast concrete pipe

The prestressed precast concrete pipe was a precast concrete hollow pipe prestressed by prestressing rebars (Fig. 3); the prestressing device was from JianHua Pipe Plant, and the procedure followed standard JGJ/T 406–2017 [10]. All details of the pipe and its prestress are shown in Fig. 3.

2.2.2. Specimen and connection design details

After transporting the pipe to the site, the specimens were built on site. The two rigid connections introduced in this paper connect PCCPCCs with foundations and/or joints in the lateral-force-resisting system such as moment-resisting frames and bridges. Usually, the first floor is critical under lateral local in a multiple-story structure due to the longest distance between the foundation and the inflection point. Inflection points of those columns on the first floor are located at around 2/3 of the columns' height (i.e., 2 m of the widely used 3 m column). Thus, the length of PCCPCCs in specimens was designed to be 2 m to study the mechanical performance of a length from the foundation to the inflection points of PCCPCCs.

Figs. 4 and 5 shows the details of specimens under these two rigid connections. The pipe was precast, which was assembled with the cast-in-situ concrete core to form the column (PCCPCC). Besides, the cast-in situ concrete foundation was heavily reinforced to prevent any potential failures, and the top surface of the PCCPCC was covered by a cast-in-situ concrete block for loading. The assembly procedures of the column, and the rest of cast-in-situ concrete component of the specimen were as follows.

2.2.2.1. Reinforcing-cage connection (RC connection). As indicated in Fig. 4, connection rebars and connection stirrups were used to form the reinforcing-cage connection, after which the reinforcing cage of PCCPCC was placed longitudinally into the foundation's center. After 7 days of casting the concrete foundation on site, the concrete foundation surface was chipped to increase the bonding between the foundation and PCCPCC. The mortar was then poured on the surface of the foundation to connect the precast concrete pipe to the cast-in-situ concrete foundation, after which the core of PCCPCC was filled in with cast-in-situ concrete.

2.2.2.2. Welded-plate connection (WP connection). As Fig. 5 displays, 11 evenly placed normal steel bars were plug-welded to a circular hollow steel plate (connection plate) vertically. The connection plate was then placed in the foundation; meanwhile, the 11 steel bars were anchored into the foundation to increase the strength of the connection. After 7 days of the concrete cast of the foundation, the pipe was placed above the foundation's center. The two steel plates were welded together, and in-situ concrete was cast into the pipe core.

The precast pipes, core concrete, mortar, rebars, stirrups, and steel plates were purchased from local suppliers. Concrete and mortar's compressive strengths were tested according to GB/T 5223.3–2017 standard [12], as shown in Table 2. Table 3 illustrates the tensile strengths of reinforcements. The tensile strengths of the connection plate and the connection/anchored reinforcements were tested according to GB/T 228.1–2021 standard [13]. The tensile strengths of the pipe-prestressed rebar and pipe-plate were provided by standard GB/T 50152-2012 [14]. The manufacturer provided the ultimate tensile strength of pipe-stirrups.

2.2.3. Axial loading design

As shown in Table 1, axial loading was applied to evaluate how PCCPCCs perform under the two connections when exposed to different loading conditions after the design of two different types of rigid connections. The mechanical performance of specimens was

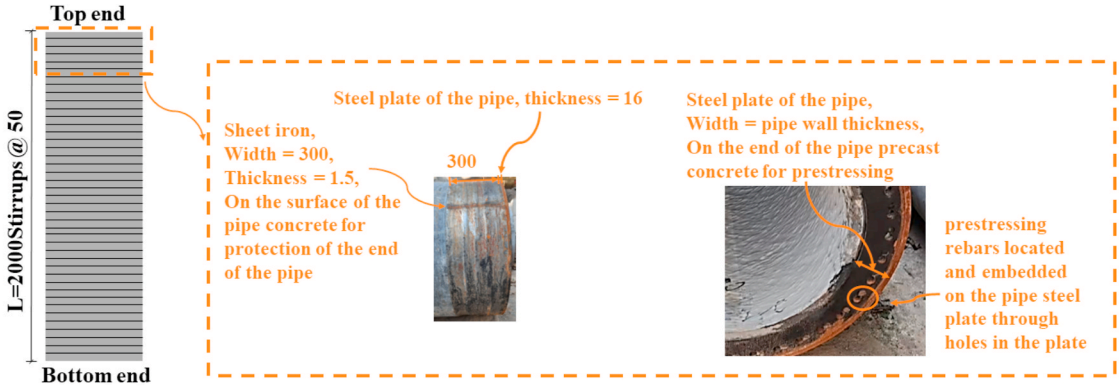

(a) Details of pipe iron sheet, pipe steel plate, and stirrups (the end of pipe attached with the steel plate was placed on the upsides for the reinforcing cage connection, whereas it was placed towards the downsides for the welded plate connection) unit in mm

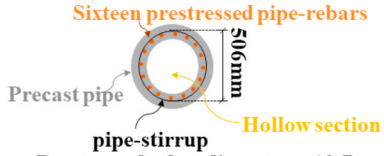

Prestressed rebar diameter = 10.7mm
Stirrup diameter = 5mm
Pipe outer diameter = 600mm, wall thickness = 130mm
Prestress per rebar = 989.8 MPa
Yield stress per rebar = 1280 MPa
Ultimate stress per rebar = 1420 Mpa
The ratio of prestress to yield stress = 0.77
The ratio of prestress to ultimate stress = 0.67

(b) Pipe cross-sectional details (outer diameter of pipe = 600 mm)

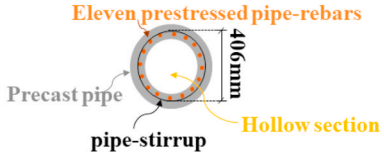

Prestressed rebar diameter = 10.7mm
Stirrup diameter = 5mm
Pipe outer diameter = 500mm, wall thickness = 100mm
Prestress per rebar = 989.8 MPa
Yield stress per rebar = 1280 MPa
Ultimate stress per rebar = 1420 Mpa
The ratio of prestress to yield stress = 0.77
The ratio of prestress to ultimate stress = 0.67

(c) Pipe cross-sectional details (outer diameter of pipe = 500 mm)

(d)

Fig. 3. Details of the precast pipe design. (Unit in mm) (a,b,c) Details of the prestressed precast pipe, (d) the prestressed precast pipe in the plant.

investigated using extreme axial loads of 3000 kN and 500 kN, which were the maximum and minimum design load in the project. RC1 and RC2 had the same cross-sectional area but under different axial loads, which aimed to investigate how the axial load influences the mechanical performance of PCCPCCs under the reinforcing-cage connection. RC3, WP4, and WP5 were in the same cross-section size,

Table 1
Details of experimental design.

Specimens	Connection types	Axial loading[a] (kN	Specimen size[b] (mm	
			D	t
RC1	RC Connection	3000	600	130
RC2	RC Connection	500	600	130
RC3	RC Connection	3000	500	100
WP4	WP Connection	3000	500	100
WP5	WP Connection	500	500	100

[a,b]: 3000 kN is the maximum loading, and 500 kN is the minimum loading where PCCPCCs are designed to support in the project; the range of axial loading, diameter and thickness selected in Table 1 covers all the design scenarios indicated by the Jianke Architectural Design Institute of Guangdong Province. Therefore, the experiments have already considered and validated all project design parameters.

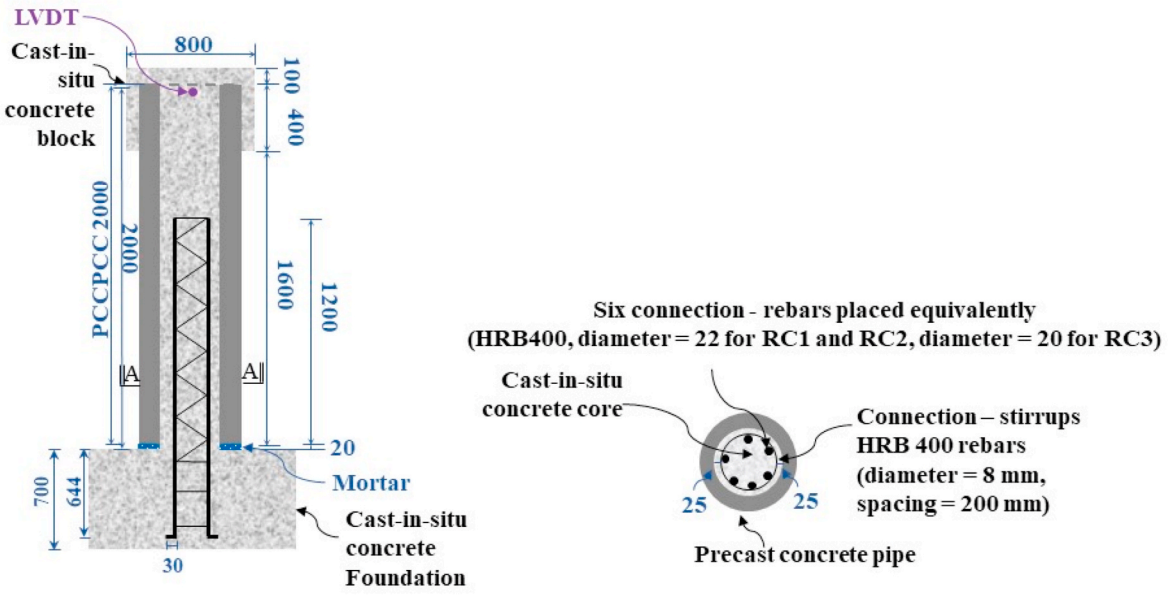

Fig. 4. Schematic drawing of specifications of specimen under RC connection (unit in mm).

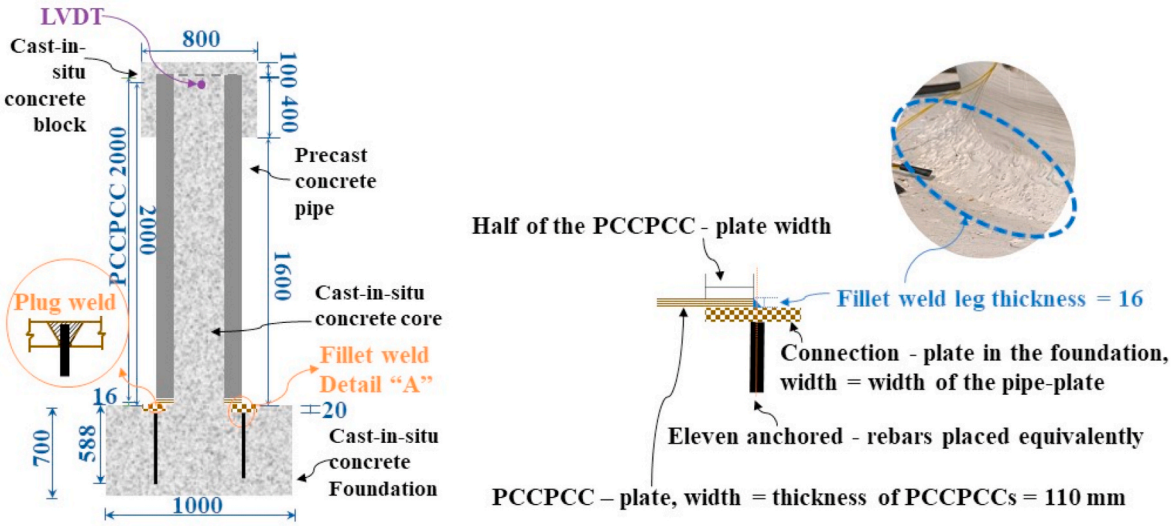

Fig. 5. Schematic drawing of specifications of specimen under WP connection (unit in mm).

Table 2
Material properties of concrete of cube specimens (150x150 × 150mm).

Concrete types	Tested concrete compressive strengths $f_{cu,k}$ (MPa)	Design concrete compressive strengths f_c (MPa) [15]
Concrete core, concrete block, and foundation (C30, cast-in-situ)	33.3	14.3
Precast concrete (C80)	89.4	35.9
Mortar (C60, cast-in-situ)	73.1	27.5

where RC3 and WP4 were under the same load to experiment with the performance of two different connections (the reinforcing-cage connection and welded-plate connection) under the same axial load. Different axial loads were applied to WP4 and WP5 to evaluate the mechanical performance of PCCPCCs under the welded-plate connection when different loads were applied.

In GB 50010-2010 [24], the axial compression ratio (ACR) is determined using Equ. (1), with a sample calculation for RC3 (Equ. (2)).

$$\mathrm{ACR} = \frac{P}{A_{pipe} \times f_{c,pipe} + A_{core\ conrete} \times f_{c,core\ concrete}} \tag{1}$$

Where P represents the designed axial load; A_{pipe} and $A_{\mathrm{core\ concrete}}$ are the cross-sectional areas of the pipe and core concrete, respectively; $f_{c,\ pipe}$ and $f_{c,\ core\ concrete}$ stand for the designed concrete compressive strength for the pipe and the core concrete, respectively.

$$\mathrm{ACR} = \frac{30000 \times 10^3 N}{(34774 \times 35.9 + 61575 \times 14.3)\mathrm{N}} = 0.54 \tag{2}$$

The areas of the cross-section of precast pipe and core concrete are 134774 mm^2 and 61575 mm^2 for RC3. The ACR of RC3 is 0.54 based on Equ. (1) and the designed concrete compressive strength f_c in Table 2. ACR can thus be determined for all specimen designs as: RC1 (0.37), RC2 (0.06), RC3 (0.54), WP4 (0.54), WP5 (0.09).

3. Loading application

3.1. Experimental boundary conditions and set-up

As shown in Fig. 6 (a), the top of the specimen has a free boundary condition, allowing the specimen to deform and rotate. According to JGJ/T 101–2015 [17], the experimental setup and equipment were decided, as shown in Fig. 6 (b). The equipment consists of a Static Materials Test Systems (MTS) actuator and a hydraulic jack to apply lateral and axial loads to specimens. A 1500 kN capacity MTS actuator controlled the cyclic lateral loads, while the constant axial load was applied to the specimens by a hydraulic jack with a maximum load capacity of 3000 kN. A liner variable differential transducer (LVDT in Fig. 6 (b)), which was used to detect and record lateral displacement at a height of 2 m, was attached to the surface of the concrete block, while the axial load was detected by the load cell under the hydraulic jack. Fig. 6 (b) also shows that the foundation of specimen was fixed in both lateral and horizontal directions to avoid any displacement and rotation to maintain as the fixed end boundary. Additionally, the lateral loading directions are shown in Fig. 6 (c).

3.2. Experimental protocol and procedure

Experiments were conducted based on the JGJ/T 101–2015 [17]. As shown in Fig. 6(d), cyclic loading was performed, and three cycles formed one stage. The specimens were under a combination of load-displacement control. The loading procedure follows: (1) axial load was applied to the specimen within a loading cycle starting at ±30 kN; (2) specimens were initially under lateral load controlled with an increment of 30 kN; (3) with the gradual increase of lateral loading, the experimental yield displacement Δy (referring to the free-end displacement in Fig. 6 (a) and the values in Table 4) was finally observed and determined on the recorded lateral load-displacement curve on-site during experiments; (2) specimens were under displacement-control after yielded with the increment of $\pm\Delta_y$. The experiment ended if the specimen was observed as a severe failure. The failure criterion of the RC connection in this research was regarded as the delamination between the PCCPCC and the foundation, while the failure criterion of the WP

Table 3
Material properties of reinforcements.

Reinforcement types	Ultimate tensile strengths (MPa)	Yield strengths (MPa)
Pipe-prestressed rebars	1420.0 [14]	1280.0 [14]
Pipe-stirrups	600.0	–
Connection-stirrups (diameter = 8 mm, HRB 400)	598.5	446.8
Connection-rebars, anchored-rebars (diameter = 20 mm, HRB 400)	636.5	443.0
Connection-rebars (diameter = 22 mm, HRB 400)	616.4	445.2
pipe-plate (Thickness = 16 mm, Q235B)	370.0 [16]	235.0 [16]
Connection - plate (Thickness = 20 mm, Q355)	511.2	383.0

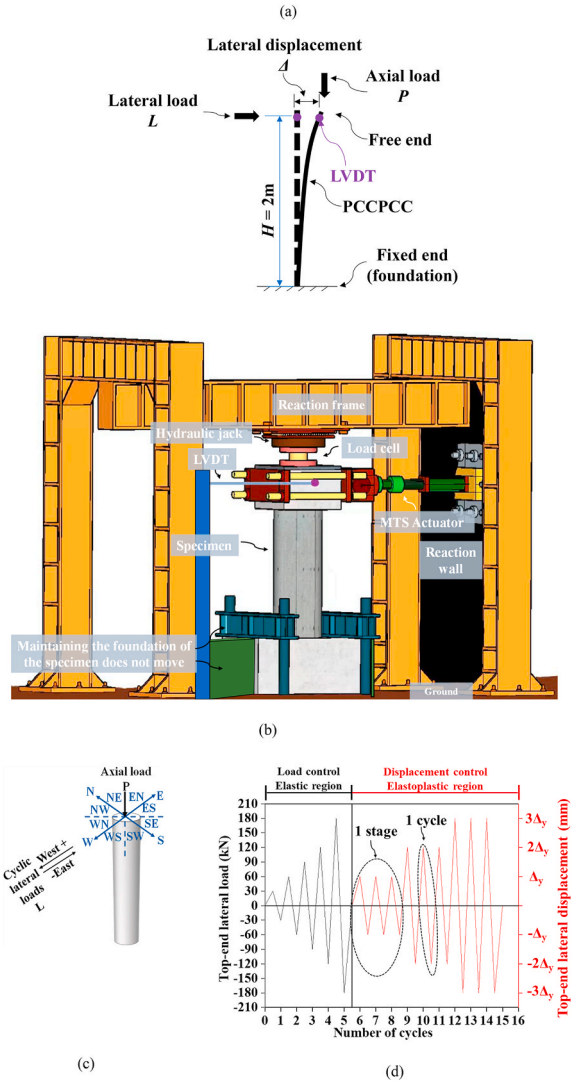

Fig. 6. Details of experiment design. (a) Details of boundary conditions, (b) Details of experimental set-up, (c) Lateral loading directions, (d) Experiment lateral loading protocol (Δ_y: yield displacement when specimen is yielded; the values used in experiments are shown in Table 5).

Table 4
Experimental yield displacement (Δ_y).

	RC1	RC2	RC3	WP4	WP5
$\pm\Delta_y$[a] **(mm)**	±5.0	±6.0	±6.0	±10.0	±12.0

[a] Experimental Δ_y was where the inflection point was observed on the hysteresis curves in experiments. The symbol "+" and "-" represent the opposite and negative directions.

specimens was the lateral loads decreased below 50 % of the maximum lateral load.

The detailed experimental procedures are as follows. RC1 was under loading control (cyclic loading) from ±30 to ±180 kN (6 stages total, increment of 30 kN), after which the specimen became displacement-controlled where increment was Δ_y equalling ±5 mm until failure. Loading was set from ±30 to ±90 kN (3 stages, increment of 30 kN) for RC2, and it changed to be displacement controlled; it increased with the increment of Δ_y equalling ±6 mm until failure. RC3's load-controlling was from ±30 to ±120 kN (4 stages, increment of 30 kN), and the displacement-controlling had an increment of Δ_y equalling ±6 mm to the failure stage. WP4 and WP5 were under load controlling of ±30 to ±180 kN (6 stages total, increment of 30 kN), after which the specimen became displacement-controlled where the increment was Δ_y equalling ± 10 mm and ±12 mm, respectively, until failure.

Table 5
Acceptance criteria of drift ratio* of moment resisting frame structures and the performance of specimens at the corresponding drift ratio.

Drift ratio	Acceptance criteria of the corresponding drift ratio [19]	% of the maximum lateral load				
		RC1	RC2	RC3	WP4	WP5
±0.2 %	Remaining elastic under frequently occurred earthquakes and wind loads	Remaining elastic				
1 %	No structure collapse happened to moment frame-shear wall structures under rarely occurred earthquakes	97	N/	99	N/A	N/A
−1%		98	A[a]	100		
2 %	No structure collapse happened to moment frame structures under rarely occurred earthquakes	89	N/A	88	97	
−2%		98	96	85	100	

*The term "drift ratio" in the standard refers to the overall drift ratio of a structure story. For example, if the standard mandates the requirement at a drift ratio of 0.2 %, it's for the story's drift ratio, not the column's drift ratio. Since the drift ratio of a story is the sum of the drift ratio of the beam, the column, and the joint at that story. Hence, when a story attains a drift ratio of 0.2 %, the column's drift ratio should be smaller than 0.2 % at this moment. To ensure maximum safety, we assign the story drift ratio requirements to the column, which is a conservative approach.

[a] N/A means the specimen has not yet reached the maximum lateral load.

4. Experimental results and discussions

4.1. Experimental observations and failure modes

Concrete cracking is a crucial scenario to be analysed. For example, in the assessment of the severity of reinforced concrete bridges, concrete cracking is regarded as one of the primary indicators of reinforced concrete bridge deterioration [18]. The horizontal cracks were observed at tension side, due to the moment caused by lateral loads and expanded horizontally. For RC connection, the horizontal cracking occurred at the mortar interface not column, the horizontal cracking only happened to columns under WP connection (Fig. 7). Fig. 7 also shows that vertical cracks and concrete spalling were observed at the bottom of PCCPCC and happened at compression side of the columns.

When the specimen was under load control, all RC specimens were in good condition without any damage. When specimens were initially controlled by the yield displacement Δy, a slight horizontal crack first occurred between the interface of mortar and precast concrete pipe of the column among three specimens, and propagation expanded horizontally and gradually with the increase of lateral loading. Then the vertical cracks and precast concrete spalling of PCCPCC happened. Finally, the mortar was crushed, and the PCCPCC was delaminated from the foundation. ACR (axial compression ratio) is a major factor that affects concrete spalling. In detail, RC3 with a higher ACR (0.54) experienced a larger amount of concrete spalling, leading to the crushing of concrete cover and the exposure of pipe-stirrups (Fig. 7). But for RC1 and RC3 under a smaller ACR, the concrete spall occurred only at a small region. Damage only occurred at the bottom end of PCCPCCs due to the maximum stress it was exposed to.

WP4 and WP5 were in good condition without any damage under load controlled. For both WP4 and WP5, the slight horizontal crack began at the bottom span of PCCPCC above the iron sheet (Fig. 3) and propagated horizontally when they were exposed to the displacement control gradually, which indicates that the sheet iron can protect the bottom of the column. Then vertical cracks formed, and concrete cover spalling happened, leading to the exposure of stirrups. Such severe cracking and spalling were because WP4 was under a large ACR. No vertical cracks happened to the PCCPCC of WP5 since it was under an extremely low ACR. Besides, only a tiny amount of surface concrete spalling was observed for WP5. The remaining part of all WP specimens was in good condition.

The horizontal cracks only occurred in columns under the WP connection instead of the RC connection. This is because the pre-stressing rebars in the precast concrete were anchored to the foundation so that the rebars were under tension for the WP connection, while the rebars in the precast component were not anchored to the foundation in the RC connection. Generally, all specimens were in full axial load capacity, and no collapse happened to each specimen.

4.2. Backbone curves and hysteresis curves

4.2.1. Lateral load capacity

Based on the backbone curves in Fig. 8 and hysteresis curves in Fig. 9, it is observed that each specimen was in the elastic deformation phase before Δ_y. During elastic deformation, the lateral load and displacement slope increased linearly. However, after Δ_y, all specimens exhibited plastic behavior, with the lateral load continuing to increase until it reached its maximum capacity. Eventually, each specimen experienced a decrease in its lateral load after reaching the maximum capacity.

Fig. 8 compares the connection type and ACR for different specimens. When comparing RC1 and RC2, it is observed that RC1, with a higher ACR, experienced a more significant decrease in its lateral load after reaching the maximum load than that of RC2. This suggests that the higher axial load accelerates the deterioration of PCCPCC under RC connection and decreases its capacity to withstand lateral loads. Additionally, the backbone curve comparison of RC1 and RC2 shows that an increasing ACR decreases the lateral displacement at failure, indicating that a higher axial load reduces plastic deformation. Comparing two specimens under the same connection (RC1 vs. RC2, WP4 vs. WP5) shows that the specimen with a higher ACR experiences a larger maximum lateral load. When comparing two specimens under the same axial load but different connections (RC3 vs. WP4), it is noted that WP4 had a steeper decreasing slope than RC3, but the former's maximum lateral load was higher than the latter. This suggests that PCCPCC under WP connection has a stronger capacity to withstand lateral loads but has a steeper decrease. This is because of the severe concrete crushing on WP4.

In Fig. 9, it is seen that the hysteresis curve of the specimen with a lower ACR is more pinched (RC1 vs. RC2, WP4 vs. WP5), indicating that it has a lower ability to dissipate energy during the cyclic loading. Fig. 9 illustrates that the horizontal crack of RC1

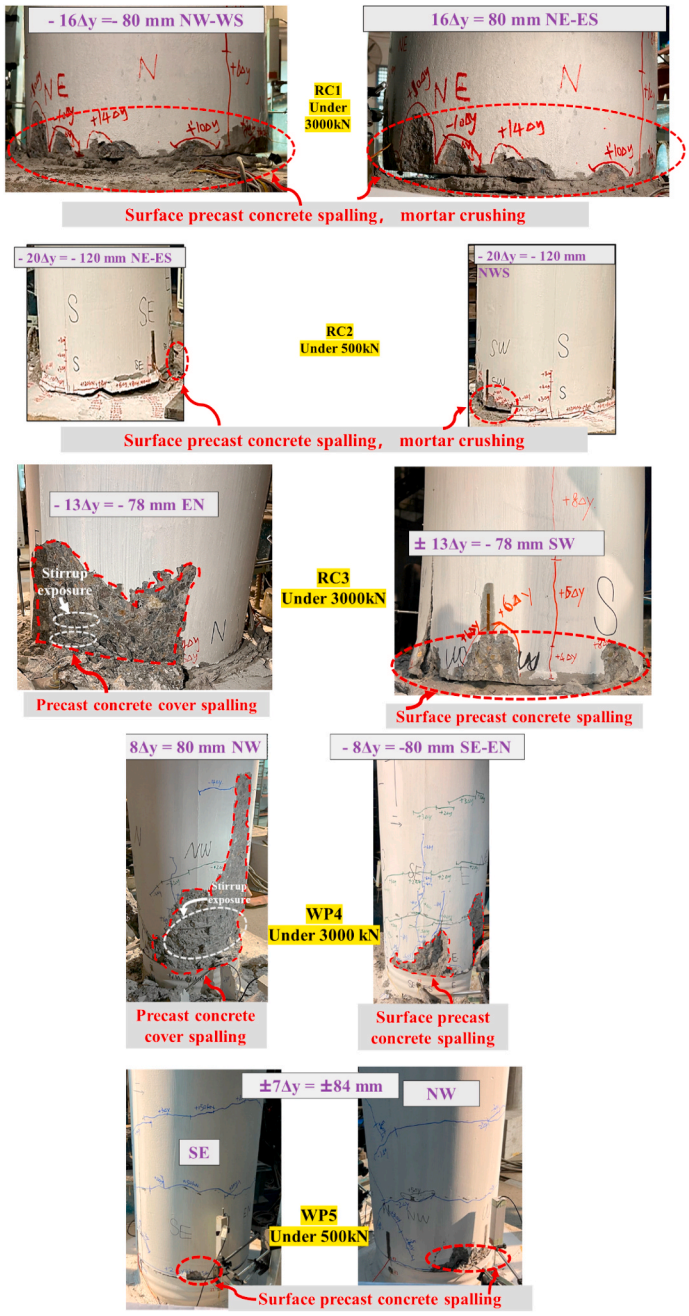

Fig. 7. Failure patterns of RC1, RC2 RC3, WP4 and WP5.

occurred at a drift ratio of 0.25 % in both negative and positive directions. However, the maximum lateral load was reached at the drift ratio of +0.9 % and −1.75 %. For the remaining specimens, the horizontal cracks of RC2, RC3, WP4, and WP5 occurred at the drift ratio of ±0.3 %, ±0.3 %, ±0.5 %, and ±0.6 %, respectively. Nevertheless, the maximum lateral load of each corresponding specimen was at the drift ratio of +3.7 % & −1.2 %, +0.8 % & −1.2 %, +1.4 % & −2.0 %, and +2.3 % & −2.4 %.

Cracking is the signal of the specimen becoming plastic. The horizontal cracking occurred to the column under the welded-plate connection; the horizontal cracking only occurred at the mortar interface when the specimens were under the RC connection. The horizontal crack was very small at the beginning. Meanwhile, the lateral capacity increased without any loss in the axial capacity. As the lateral loads increased, the horizontal crack propagated gradually. After reaching the maximum lateral capacity, the lateral load decreased gradually. This phenomenon indicates that the column is in ductile failure mode, which is good for structural applications. Ductile failure of the column has a signal when it turns into plastic and deforms for a period under plastic performance before its failure. This gives safety instructions to retrofit the columns before any damage occurs, avoiding safety accidents.

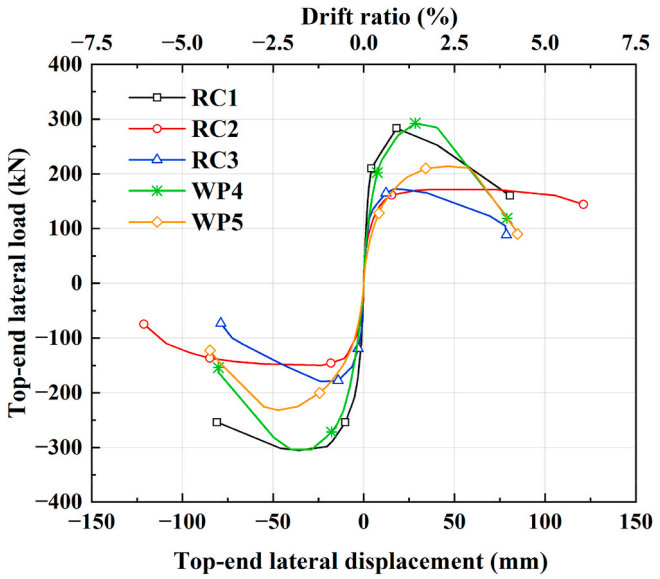

Fig. 8. Backbone curves of RC1, RC2, RC3, WP4 and WP5.

Table 5 indicates the acceptance criteria for structures when an earthquake happens. Each specimen had a good performance at the specified drift ratio. Specimens all remained elastic at the drift ratio of ±0.2 %. At the drift ratio of ±2 %, no severe failure or significant decrease of lateral load happened to specimens; only small cracks or slight surface concrete crushing occurred. All specimens meet acceptance requirements; therefore, the new connection designs can be used for various construction projects.

4.2.2. Moment capacity

As previously mentioned, the area under the largest stress was the bottom cross-section. This can also be proved from the failure patterns shown in Fig. 7. Moment at the bottom cross-section of PCCPCCs is determined in Equ. (3) based on the measured displacement Δ in Fig. 6(a).

$$M_{p-\Delta} = P \times \Delta + L \times H \tag{3}$$

Where P is the axial load, Δ refers to the top-end lateral displacement of the specimen, L stands for the top-end lateral load, and the height of the specimen is H.

RC1 has a 0.7 % and 4.5 % decrease and increase at the moment in the positive and negative directions (explanation of directions shown in Fig. 6 (c)) at the failure point. For RC2, moments in both the positive and negative directions at the failure point decreased by 8.2 % and 3.3 %, respectively. For RC3, an increase of 13.0 % and a decrease of 10.1 % were observed in the positive and negative directions. A reduction of 3.1 % and 3.0 % in the positive and negative directions, respectively, were obtained for WP4. Finally, for WP5, the moment decreased by 5.3 % and 4.7 % in the positive and negative directions, respectively. Results show that the moment at the bottom cross-sectional area of PCCPCCs only decreased by about 10 % or less.

Fig. 8 shows a dramatic reduction of lateral load between its peak failure and failure point; however, such dramatic reduction is not reflected on the calculated moment ($M_{P\text{-}\Delta}$) because of P-Δ effect. This is also supported by Fig. 7, which shows that failure only occurs at a regional area for all specimens. Therefore, specimens remained at sufficient moment capacity, regional damage, and full axial load capacity, which proves that PCCPCCs under these two rigid connections did not face a dramatic loss on its mechanical performance when they were supposed to cyclic lateral loads.

4.2.3. Cracking moment M_{cr} of PCCPCCs

As mentioned in Section 4.2.1, cracking is the critical scenario in this study, which indicates that PCCPCCs changes from elastic into plastic performance. Also, as observed before in Section 4.1, horizontal cracking initially occurred between mortar and precast concrete for specimens under RC connection, while horizontal cracking firstly occurred at precast concrete for specimens under WP connection. In accordance with the concrete principles [20], the theoretical results (Equ (4) (5), and Table 6)., are calculated using a conservative concrete standard tensile strength f_{tk} which is smaller than the actual value so that the theoretical results should be smaller than the experimental ones. Moreover, compared RC3 with WP4, which were in the same axial load and cross-sectional area, WP4 with prestress has a higher M_{cr}, which indicates that the prestress can enhance M_{cr}. Both theoretical and experimental M_{cr} have the same trend that under same conditions the higher axial load has the higher M_{cr} (RC1 vs. RC2, WP4 vs. WP5). Additionally, the shear strength of the prestressed precast pipe used in RC1, RC2 was 546 kN according to standard JGJ/T 406–2017 [10], the maximum lateral load among RC1 and RC2 was only 304.9 kN in Fig. 9 (a); the shear strength of the pipe used in RC3, WP4, and WP5 was 380 kN, the maximum lateral load among these three specimens was only up to 303.6 kN in Fig. 9 (d). Therefore, specimens failed due to

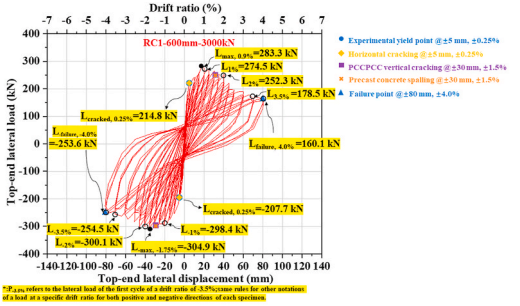

(a)

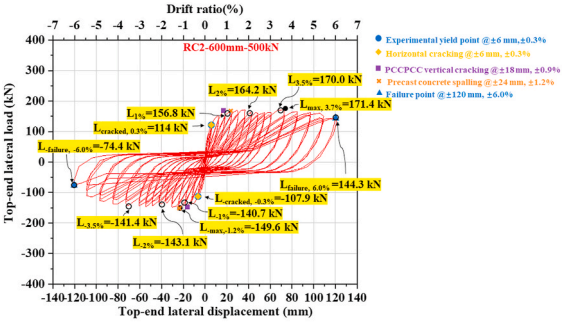

(b)

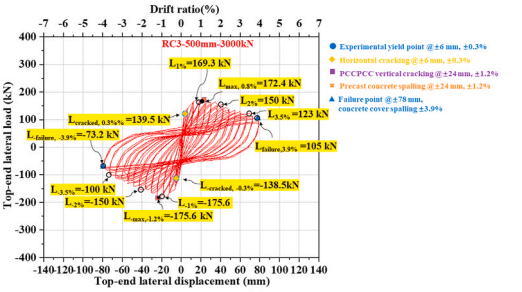

(c)

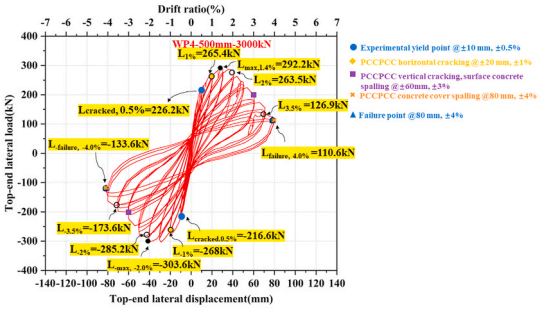

(d)

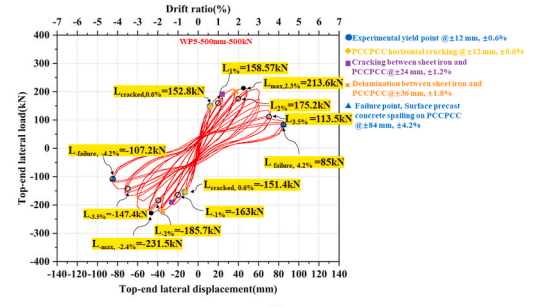

(e)

(caption on next page)

Fig. 9. Hysteresis curves of RC1, RC2, RC3, WP4 and WP5. (a) Hysteresis curve of RC1, (b) Hysteresis curve of RC2, (c) Hysteresis curve of RC3, (d) Hysteresis curve of WP4, (e) Hysteresis curve of WP5.

moment, not shear, as hollow pipes without a concrete core and connection have much higher shear strength than the maximum lateral loads specimen againsted in experiments.

Specimens under RC connection (RC1, RC2, and RC3), where prestressing rebars were not anchored into foundation, prestressing rebars were not in tension, the math is only based on its longitudinal connection-rebars. Equ. (4) is used to calculate the theoretical M_{cr} for specimens under RC connection.

$$M_{cr} = \left(\frac{N}{A} + \gamma f_{tk}\right) S \tag{4}$$

Where N is the axial load, A is the equivalent area of the cross section of the composite column's bottom, γ is the impact coefficient of section modulus, f_{tk} is the concrete standard tensile strength (f_{tk} of C60 concrete = 2.85 MPa for mortar, f_{tk} of C80 concrete = 3.11 MPa according to standard GB 50010-2010 [15]), and S is the section modulus of the cross section of the composite column's bottom.

WP connection, where prestressing rebars were anchored into foundation, prestress rebars are in tension. Equ. (5) is used to calculate the theoretical M_{cr} for specimens under the WP connection.

$$M_{cr} = \left(\frac{N}{A} + \gamma f_{tk} + \sigma_p\right) S \tag{5}$$

Where σ_p is the stress of prestress in precast concrete which 6.59 MPa in accordance with code JGJ/T-2017 [10].

4.3. Energy dissipation

Hysteretic energy is crucial to estimate when designing energy-based approaches and assessing potential damage to structures [21], which refers to the lost energy in inelastic performance during seismic activity [22].

Equ. (6) from the American Concrete Institute code ACI 374.1-05 [23] standard uses the relative energy dissipation ratio (β) to assess the performance of dissipating hysteretic energy. This index is to measure the ratio between the actual and ideal amount of energy dissipating during seismic tests. ACI 374.1-05 requires that energy dissipation ratio should be 12.5 % or higher at a drift ratio of 3.5 %, and all the specimens in this study meet the requirement, as proven in Fig. 10.

$$\beta = \frac{A_h}{(E_1 + E_2)\left(\theta_1^{'} + \theta_2^{'}\right)} \tag{6}$$

$$\theta_1^{'} = \Delta_{P,+} - \frac{L_{p,+}}{K_{initial,+}} \tag{7}$$

$$\theta_2^{'} = \Delta_{P,-} - \frac{L_{p,-}}{K_{initial,-}} \tag{8}$$

where A_h is the area of the hysteresis loop at the specific drift ratio, and E_1 and E_2 represent the absolute values of this loop's peak lateral loads in the positive and negative directions, respectively. Moreover, $\theta_1^{'}$ and $\theta_2^{'}$ are the values of Equ. (7) and (8), where the "+" and "-" stand for the positive and negative direction of this loop, respectively; Δ_p and L_p are the displacement and lateral loads at the peak of this loop, respectively; $K_{initial}$ is the initial stiffness which can be regarded as the stiffness of the first loop.

A higher ACR leads to a higher energy dissipation capacity for specimens at the same connection (RC1 vs. RC2, WP4 vs. WP5). Under the same ACR, the RC specimen (RC3) performed better than the WP specimen (WP4), as seen in Fig. 9, where the hysteresis loop of the RC3 area is larger than that of WP4. This is because severe concrete crushing happened to WP4.

4.4. Ductility

Ductility, represented by the ductility factor (μ), is another key parameter to evaluate the mechanical performance of structural elements and connections under earthquakes [24]. The coefficient is calculated as Equ. (9) [25].

$$\mu = \frac{\Delta_u}{\Delta_y} \tag{9}$$

where Δ_y is the yield displacement as mentioned before; and Δ_u is the ultimate displacement, which is the corresponding horizontal displacement when the lateral load decreases to 85 % of the maximum lateral load at the maximum point [26].

Table 7 shows the ductility coefficient based on the yield strength determined by three commonly used methods and the average ductility coefficient (μ_{avg}) shown in Equ. (10).

$$\mu_{avg} = \frac{\Delta_{u-} + \Delta_{u+}}{2} \tag{10}$$

As shown in Table 7, the general yield moment method obtains the highest ductility coefficient among all specimens when

Table 6
Comparison between theoretical and experimental cracking moment.

	Theoretical cracking moment (kNm)	Experimental cracking moment (kNm)
RC1	385.51	+429.60, −415.40
RC2	164.36	+228.00, −215.80
RC3	244.63	+279.00, −277.00
WP4	336.73	+425.40, −433.20
WP5	171.37	+305.60, −302.80

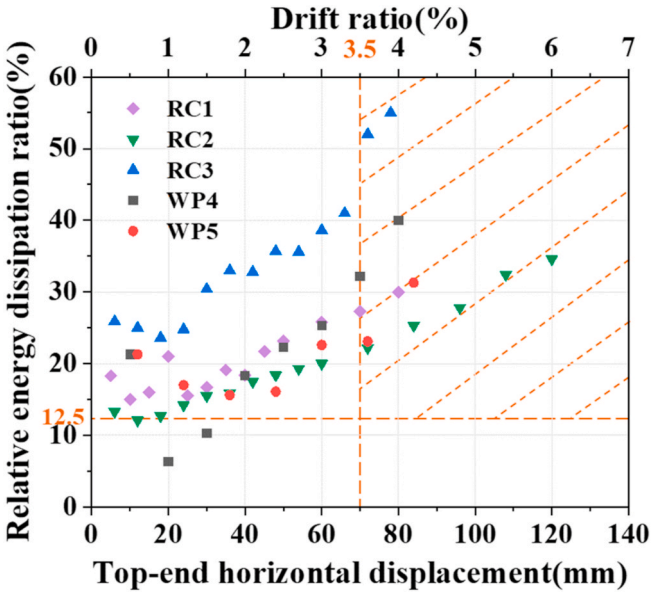

Fig. 10. Comparison of energy dissipation ratio of RC1, RC2, RC3, WP4 and WP5.

compared to the other two methods. By comparing the average ductility coefficient in Tables 7 and it is indicated that (1) the RC connection performed better in ductility than the WP connection under the same ACR (RC3 vs. WP4); (2) comparison between RC1 and RC2 illustrates that the increase in ACR reduceed the ductility of the RC specimen; (3) comparing WP4 with WP5, ACR increased 6 times (0.09–0.54), but the ductility coefficient of these two specimens does not have an obvious difference. WP4 and WP5 have similar ductility coefficients; however, WP5 performed a larger ultimate displacement than WP4 (Fig. 11) due to its lower ACR. It indicates that lower ARC can lead to a better performance in plastic deformation.

The ductility coefficient of a ductile structural member should be no less than 3 according to Caltrans Seismic Design Criteria [28], which is achieved by all specimens (based on the average value). It indicates that PCCPCCs under these two connections are ductile and can be adopted in moment-resisting frames or bridges.

5. Conclusions

Through conducting a series of experimental tests on five full-scale specimens, this study demonstrates the sufficient mechanical performance of PCCPCCs with reinforcing-cage and welded-plate connections under cyclic lateral loading and constant axial loading.

Table 7
Comparison of ductility based on three methods of specimens under different types of rigid connections and ACR.

Specimens	Park's method [25] (Park coefficient = 0.75) (P)			Equivalent energy method [25] (EE)			General yield moment method [27] (G)		
	Ductility coefficient (μ)								
	+	−	Average	+	−	Average	+	−	Average
RC1	7.16	7.23	7.20	5.56	6.95	6.26	10.66	12.23	11.60
RC2	13.18	11.16	12.17	12.41	6.86	12.13	39.06	9.82	37.70
RC3	8.58	6.82	7.70	7.58	6.56	7.07	13.06	9.82	11.44
WP4	3.98	3.85	3.92	3.78	3.67	3.73	6.38	5.82	6.10
WP5	3.47	2.87	3.17	3.53	2.97	3.25	7.10	5.58	6.34

The following are some major findings.

1) For surface damage observation, horizontal cracks were only observed on the tensile side of PCCPCCs with welded-plate connections. For the rest of the specimens under the reinforcing-cage connection, horizontal cracking occurred at the mortar interface but not the column. Concrete cover spalling was observed in RC3 and WP4 under a high axial compression ratio (ACR) of 0.54. However, only minor surface concrete spalling was found in other specimens. Moreover, among all five specimens, no collapse or loss in axial load capacity was observed in any specimen.
2) For elasticity and load retention, all the specimens can generally maintain their elasticity up to a drift ratio of 0.2 %, and the reduction in lateral load at a 2 % drift ratio was below 15 % of the peak lateral load for each specimen. The results comply with GB50011-2010 [19] which suggests that the structures remain elastic during frequently occurred earthquakes, and can against collapse during rarely occurred earthquakes.

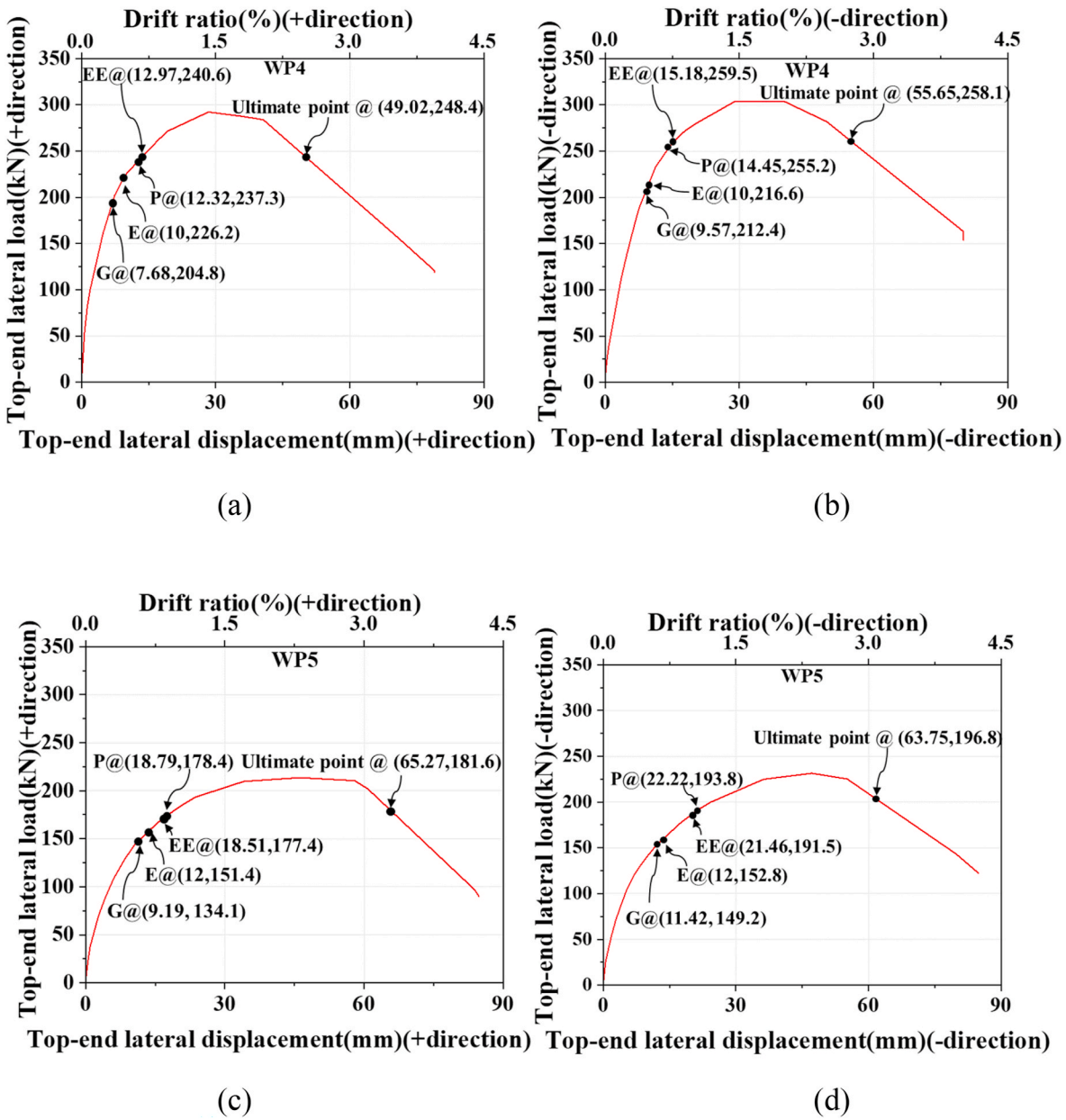

Fig. 11. Yield, and ultimate points of WP4 and WP5. (a) Yield, and ultimate points in the positive direction of WP4, (b) Yield, and ultimate points in the negative direction of WP4, (c) Yield, and ultimate points in the positive direction of WP5, (d) Yield, and ultimate points in the negative direction of WP5 (E stands for the experimental yield point).

3) For moment capacity, despite some decrease in lateral load capacity, the moment capacity at the specimens' bottom end, the most critical cross-section, remained nearly unaffected, confirming their consistent mechanical performance for applications in the lateral-force-resisting system.
4) For energy dissipation, the relative energy dissipation ratio for all specimens surpassed the 12.5 % threshold specified in ACI 374.1-05 [23] at a drift ratio of 3.5 %, indicating satisfactory energy dissipation capacity.
5) For ductility, the specimens with reinforcing-cage connections demonstrated a ductility greater than 7, while those with welded-plate connections had a ductility exceeding 3. Both configurations showcase adequate ductility for application in lateral force-resisting systems.

In summary, each specimen under these two rigid connections shows sufficient mechanical performance against combined cyclic lateral loads and constant axial load, which indicates that PCCPCCs under the reinforcing-cage connection and welded-plate connection are satisfactory to be adopted in lateral force-resisting systems such as moment-resisting frames and bridges.

CRediT authorship contribution statement

Caiwei Xu: Conceptualization, Data curation, Formal analysis, Investigation, Methodology, Resources, Visualization, Writing – original draft, Writing – review & editing. **Le Li:** Formal analysis, Supervision, Visualization, Writing – review & editing. **Saeed Miramini:** Supervision. **Lihai Zhang:** Supervision, Validation, Visualization, Writing – review & editing.

Declaration of competing interest

The authors declare that they have no known competing financial interests or personal relationships that could have appeared to influence the work reported in this paper.

Data availability

Data will be made available on request.

Acknowledgments

The authors would like to thank The University of Melbourne and Guangdong Jianke Architecture Design Institute Co., Ltd. For their supports.

References

[1] R.W.M. Wong, B.P.Y. Loo, Sustainability implications of using precast concrete in construction: an in-depth project-level analysis spanning two decades, J. Clean. Prod. 378 (2022) 134486.
[2] Q. Xu, Structural Design of Precast Concrete Structures, 2017.
[3] C. Xu, D. Chen, S. Miramini, X. Liu, W. Xu, L. Zhang, Experimental fire performance assessment of a new type of prestressed composite circular precast concrete columns, Eng. Struct. 278 (2023) 115509.
[4] R. Ma, J. Xia, H. Chang, B. Xu, L. Zhang, Experimental and numerical investigation of mechanical properties on novel modular connections with superimposed beams, Eng. Struct. 232 (2021) 111858.
[5] B. Xu, J. Xia, H. Chang, R. Ma, L. Zhang, A comprehensive experimental-numerical investigation on the bending response of laminated double channel beams in modular buildings, Eng. Struct. 200 (2019) 109737.
[6] JGJ 355-2015, Technical Specification for Grout Sleeve Splicing of Rebars, 2015.
[7] X. Hu, W. Xue, Y. Lv, Experimental studies on structural performance of precast concrete shear walls with innovative UHPC-based connections, J. Build. Eng. 73 (2023) 106748.
[8] C.G. Koh, K.K. Ang, L. Zhang, Effects of repeated loading on creep deflection of reinforced concrete beams, Eng. Struct. 19 (1997) 2–18.
[9] D. Guan, R. Xu, S. Yang, Z. Chen, Z. Guo, Development and seismic behavior of a novel UHPC-shell strengthened prefabricated concrete column, J. Build. Eng. 46 (2022) 103672.
[10] JGJ/T 406-2017, Technical Standard for Prestressed Concrete Pipe Pile, 2017.
[11] GB/T14902-2012, Ready-mix Concrete, 2012.
[12] GB/T 50152-2012, Standard for Test Method of Concrete Structures, 2012.
[13] GB/T 228.1-2021, Metallic Materials-Tensile Testing-Part 1:Method of Test at Room Temperature, 2021.
[14] GB/T 5223.3-2017, Steel Bars for the Prestressing of Concrete, 2017.
[15] GB 50010-2010, Code for Design of Concrete Structures, 2015.
[16] GB 50017 - 2017, Standard for Design of Steel Structures, 2017.
[17] JGJ/T 101-2015, Specification for Seismic Test of Buildings, 2015.
[18] S. Chen, C. Duffield, S. Miramini, B. Nasim Khan Raja, L. Zhang, Life-cycle modelling of concrete cracking and reinforcement corrosion in concrete bridges: a case study, Eng. Struct. 237 (2021) 112143.
[19] GB 50011 - 2010, Code for Seismic Design of Buildings, 2016.
[20] Z. Lan, Concrete Design Principles, 2008.
[21] P. Khashaee, B. Mohraz, S. Fahim, L. Hai, G. John, Distribution of Earthquake Input Energy in Structures. NIST Interagency/Internal Report (NISTIR), National Institute of Standards and Technology, Gaithersburg, MD, 2003.
[22] A. Kazantzi, D. Vamvatsikos, A Study on the Correlation between Dissipated Hysteretic Energy and Seismic Performance, 2012.
[23] A.C. Institute, ACI 374.1-05 Acceptance Criteria for Moment Frames Based on Structural Testing and Commentary, 2014.
[24] R. Park, Ductility evaluation from laboratory and analytical testing, in: Proceedings of the 9th World Conference on Earthquake Engineering: Tokyo-Kyoto Japan, 1988, pp. 605–616.
[25] M.B. Tadi Beni, M. Madhkhan, Experimental study on two innovative ductile moment-resisting precast concrete beam-column connections, Structures 39 (2022) 559–572.

[26] F. Yu, G. Xu, D. Niu, A. Cheng, P. Wu, Z. Kong, Experimental study on PVC-CFRP confined concrete columns under low cyclic loading, Construct. Build. Mater. 177 (2018) 287–302.
[27] T. Tafsirojjaman, S. Fawzia, D. Thambiratnam, X.-L. Zhao, Behaviour of CFRP strengthened CHS members under monotonic and cyclic loading, Compos. Struct. 220 (2019).
[28] Transportation CDo, CALTRANS SEISMIC DESIGN CRITERIA, 2013, 1.7 ed.